INTECH
open science | open minds

OPEN ACCESS
ARTICLE

International Journal of Advanced Robotic Systems

Singularity Representation and Workspace Determination of a Special Class of the Gough-Stewart Platforms

Regular Paper

Baokun Li[1,2], Yi Cao[1,3,4,*], Qiuju Zhang[1] and Chuanli Wang[2]

1 School of Mechanical Engineering, Jiangnan University, Wuxi, Jiangsu Province, Jiangsu Province, China
2 School of Mechanical Engineering, Anhui University of Science and Technology, Huainan, Anhui Province, China
3 State Key Laboratory of Robotics and System, Harbin, Heilongjiang Province, China
4 State Key Laboratory of Fluid Power and Mechatronic Systems, Hangzhou, Zhejiang Province, China
* Corresponding author E-mail: caoyi@jiangnan.edu.cn

Received 04 Dec 2012; Accepted 27 Jun 2013

DOI: 10.5772/56792

Abstract The closed-loop nature of the Gough-Stewart platform generates complex singular configurations inside the workspace and makes its workspace smaller compared to the serial mechanism. It is desirable to obtain a non-singular workspace based on describing the constraint workspace and representing the singularities inside the constraint workspace. Some algorithms have been proposed by researchers to find the workspace boundary, but cannot locate the voids inside the workspace and are not applicable to the generation of a workspace with more than one zone. In this paper, the position-singularity expression in $\Re^3$ and the orientation-singularity expression in $SO(3)$ are obtained, respectively. The new algorithms of the two types of constraint workspace in $\Re^3$ and in $SO(3)$ are developed considering the limitations of the kinematic pairs. It can be shown that the singularities may exist inside the constraint workspace. Based on the singularity representation and the abovementioned constraint workspace determination, the two types of procedures of the non-singular workspace in $\Re^3$ and in $SO(3)$ are further addressed, respectively. When the moving platform translates inside the non-singular position-workspace in $\Re^3$ for a constant-orientation or rotates inside the non-singular orientation-workspace in $SO(3)$ for a given position, the mechanism is not singular. The two types of non-singular workspace representations in $\Re^3$ and $SO(3)$ can help the designers to explore the singularity-free path planning, on which our next work will be focused. The novel method of workspace determination of the mechanism can also be used for the workspace analysis of the other types of parallel mechanisms.

Keywords Parallel Mechanism, Singularity, Constraint Workspace, Non-Singular Workspace

1. Introduction

Parallel mechanisms (PMs) have become a large field of investigation during the past several decades because of

their many attributes, including large load capacities, high stiffness and stability, and good dynamic performance. However, PMs are only one type of closed-loop spatial mechanisms and their architectural nature limits their application. One of the main limitations is that the singular configuration, also called singularity, may exist inside the workspace. Generally speaking, when a PM is singular, one or more degree of freedom (DOF) of the moving platform is not restricted, which results in the end-effector gaining at least one unwanted instantaneous DOF even if all the actuators are locked. Therefore, when the PM is singular, it becomes uncontrollable. Here the unwanted DOF is instantaneous but not continuous.

Because the singularity seriously affects the performance of the PMs, it is very important to avoid the singularities within the workspace. Merlet[1] advanced an efficient algorithm to verify a trajectory for a six-DOF parallel mechanism with respect to its workspace. Dasgupta et al. [2], proposed an algorithm for finding a well-conditioned safe path inside the workspace connecting the initial pose and the end pose. Dash et al. [3], presented a singularity-free path-planning algorithm consisting of nominal path planning and local routing to avoid the singularities. Based on the screw theory, Glazunov [4], developed an approach to determine twists, which displace the PM in singularity and find out the twist-gradient, which leads the PM from singularity to general configuration "most rapidly". Arakelian et al. [5], addressed a new procedure to increase the singularity-free zone of the PM using controlling the pressure angles in the joints of the manipulator and changing the structural parameters of the legs. Saglia et al. [6], proposed that the singularity of the parallel mechanism can be eliminated using the redundant actuators. After investigating the bifurcation characteristics of the Gough-Stewart platform (GSP), Wang et al. [7], proposed a method for avoiding the turning point singularity using a disturbance function.

The GSP, which was proposed as a flight simulator in 1965 [8], is one of the most well known PMs and now is widely used in many other practices [9]. As is known to all, PMs generally have a smaller workspace than serial mechanisms, so the workspace representation, especially the non-singular workspace representation, is another important issue in the design of PMs. In addition, in order to guarantee that the PM remains far away from the singularities, maximizing the singularity-free zone is a useful method, which was addressed by Li [10] and Jiang [11]. This work will obtain the singularity expression of a special class of GSPs with two dissimilar semi-symmetrical hexagons and develop new algorithms for determining the constraint workspace in $\Re^3$ and in $SO(3)$ and the non-singular workspace in $\Re^3$ and $SO(3)$, respectively.

2. Geometry of the GSP with two dissimilar semi- symmetrical hexagons

A sketch of this special class of GSPs with two dissimilar semi-symmetrical hexagonal platforms is shown in Figure 1. The mechanism consists of a moving platform and a base platform connected via six identical SPS or SPU legs B_iC_i(i=1, 2, …, 6). Here S denotes a passive spherical joint and U denotes a passive Hooke joint, while P denotes an actuated prismatic joint. The moving platform and the base one, whose vertices are B_i and C_i(i=1, 2, …, 6), respectively, are both semi-symmetrical hexagons. A_j(j=1, 3, 5) are the intersection points of the three sides of the base platform. The meanings of the symbols P, O, β_m, β_b, R_m, R_b are as follows:

P——Geometry centre of the moving platform

O——Geometry centre of the base platform

β_m——Central angle of side B_4B_5 of the moving platform, $0°\leq\beta_m\leq120°$

β_b——Central angle of side C_1C_2 of the base platform, where $0°\leq\beta_b\leq120°$

R_m——Circumradius of the moving platform

R_b——Circumradius of the base platform.

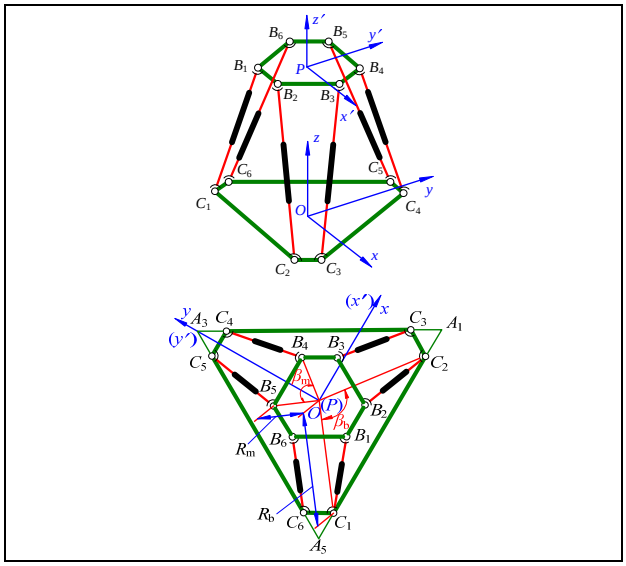

Figure 1. Sketch of the special class of the GSPs

3. Orientation representation and force Jacobian matrix

The moving reference frame P-$x'y'z'$ and the fixed reference O-xyz are attached to the moving platform and the base platform, respectively. The coordinates of six vertices, B_i(i =1, 2, …, 6), of the moving platform are denoted by $\boldsymbol{B}_i'$(B_{iX}', B_{iY}', B_{iZ}') (i=1, 2, …, 6) with respect to the moving reference frame and $\boldsymbol{B}_i$(B_{iX}, B_{iY}, B_{iZ}) (i=1, 2, …, 6) with respect to the fixed reference frame, respectively. Similarly, $\boldsymbol{C}_i$(C_{iX}, C_{iY}, C_{iZ}) (i=1, 2, …, 6) represents the coordinates of vertices C_i (i=1, 2, …, 6) with respect to the fixed reference frame. The coordinates $\boldsymbol{B}_i'$, $\boldsymbol{C}_i$ (i=1, 2, …, 6) can be obtained easily

according to the geometry of the mechanism and are not given here because of the limited space.

Here we use the unit quaternion, which is defined as $\boldsymbol{Q}=q_0+q_1\boldsymbol{i}+q_2\boldsymbol{j}+q_3\boldsymbol{k}$ ($q_0^2+q_1^2+q_2^2+q_3^2=1$), to describe the orientation of the moving platform of the GSP. This means that the moving platform is rotated by an angle $\theta=2\arccos q_0$ around the line which passes the point P and whose direction is $q_1\boldsymbol{i}+q_2\boldsymbol{j}+q_3\boldsymbol{k}$ with respect to the fixed reference frame. Furthermore, we set $q_0\geq 0$, thus the unit quaternion (q_0, q_1, q_2, q_3) gives the global parameterization of $SO(3)$ and does not suffer from singularities in parameterization [12]. The rotation matrix based on the unit quaternion representation is as follows:

$$\boldsymbol{R}=\begin{pmatrix} q_0^2+q_1^2-q_2^2-q_3^2 & 2(q_1q_2-q_0q_3) & 2(q_1q_3+q_0q_2) \\ 2(q_1q_2+q_0q_3) & q_0^2+q_2^2-q_1^2-q_3^2 & 2(q_2q_3-q_0q_1) \\ 2(q_1q_3-q_0q_2) & 2(q_2q_3+q_0q_1) & q_0^2+q_3^2-q_1^2-q_2^2 \end{pmatrix}. \quad (1)$$

Moreover, the relation between $\boldsymbol{B}_i$ and $\boldsymbol{B}_i'$ (i=1,2,…,6) satisfies

$$\boldsymbol{B}_i=\boldsymbol{R}\boldsymbol{B}_i'+\boldsymbol{P}. \quad (2)$$

where matrix $\boldsymbol{R}$ is the rotation matrix of the moving reference frame to the fixed platform using the unit quaternion to represent the orientation of the moving platform, as Equation (1) shows. The force Jacobian matrix of the mechanism can be constructed according to the principle of the static equilibrium and the screw theory, which are derived by Huang (see [13]) and not detailed here because of the limited space.

$$\boldsymbol{J}^T=\begin{pmatrix} \frac{\boldsymbol{B}_1-\boldsymbol{C}_1}{|\boldsymbol{B}_1-\boldsymbol{C}_1|} & \frac{\boldsymbol{B}_2-\boldsymbol{C}_2}{|\boldsymbol{B}_2-\boldsymbol{C}_2|} & \frac{\boldsymbol{B}_3-\boldsymbol{C}_3}{|\boldsymbol{B}_3-\boldsymbol{C}_3|} & \frac{\boldsymbol{B}_4-\boldsymbol{C}_4}{|\boldsymbol{B}_4-\boldsymbol{C}_4|} & \frac{\boldsymbol{B}_5-\boldsymbol{C}_5}{|\boldsymbol{B}_5-\boldsymbol{C}_5|} & \frac{\boldsymbol{B}_6-\boldsymbol{C}_6}{|\boldsymbol{B}_6-\boldsymbol{C}_6|} \\ \frac{\boldsymbol{C}_1\times\boldsymbol{B}_1}{|\boldsymbol{B}_1-\boldsymbol{C}_1|} & \frac{\boldsymbol{C}_2\times\boldsymbol{B}_2}{|\boldsymbol{B}_2-\boldsymbol{C}_2|} & \frac{\boldsymbol{C}_3\times\boldsymbol{B}_3}{|\boldsymbol{B}_3-\boldsymbol{C}_3|} & \frac{\boldsymbol{C}_4\times\boldsymbol{B}_4}{|\boldsymbol{B}_4-\boldsymbol{C}_4|} & \frac{\boldsymbol{C}_5\times\boldsymbol{B}_5}{|\boldsymbol{B}_5-\boldsymbol{C}_5|} & \frac{\boldsymbol{C}_6\times\boldsymbol{B}_6}{|\boldsymbol{B}_6-\boldsymbol{C}_6|} \end{pmatrix}. \quad (3)$$

Based on determinants of the mechanism's Jacobian matrices, Gosselin et al. [14], showed that singularities of PMs could be classified into three different types, inverse kinematic singularity, direct kinematic singularity and architecture singularity. The first type of singularity occurs when one length of the links is zero, i.e., $|\boldsymbol{B}_i-\boldsymbol{C}_i|=0$ (i=1, 2, …, 6), then the determinant of the Jacobian matrix $\boldsymbol{J}$ of the GSP is equal to infinity, i.e., $\det(\boldsymbol{J})=\infty$, where ∞ denotes infinity. It is easy to deal with since it leads to a very simple expression. Please refer to the explanations given by St-onge et al. [15]. This type of singularity should be avoided in the context of the design of parallel manipulators. Generally, this type of singularity mainly occurs in serial manipulators. The third type of singularity is caused by a particular architecture and can be avoided in design. For this class of the GSPs(see [16]), when $\beta_m+\beta_b=120°$, indicating that the moving platform and the base one are two similar hexagons and the corresponding vertices are connected, the mechanism is an architecture singularity. In this case, whatever the pose (position and orientation) of the GSP is, the mechanism is singular. The second type of singularity occurs when different branches of the direct kinematics problem converge and is difficult to analyse and has received much attention from many researchers. This type of singularity mainly occurs in parallel manipulators, i.e., the singularity introduced in the Introduction, that is the when a PM is singular, one or more DOF of the moving platform is not restricted, which results in the end-effector gaining at least one unwanted instantaneous DOF even if all the actuators are locked. This paper will only deal with the direct kinematic singularity analysis of the GSP, which occurs with the determinant of the Jacobian matrix $\boldsymbol{J}$ being equal to zero, i.e., $\det(\boldsymbol{J})=0$.

4. Singularity representation

Substitute Equations (1)-(2) into Equation (3) noting that $q_0=\sqrt{1-q_1^2-q_2^2-q_3^2}$, expand and rearrange the determinant of matrix $\boldsymbol{J}^T$, which equals zero when the mechanism is singular, then a general symbolic expression representing the singularity locus embedded in six-dimensional configuration space is derived

$$F(\mathscr{X}, \mathscr{Q})=0, \quad (4)$$

where $\mathscr{X}=(X, Y, Z)$ represents the position parameters and $\mathscr{Q}=(q_1, q_2, q_3)$ indicates the orientation parameters. For example, when R_b=2, R_m=1, β_b=105°, β_m=75°, X=0.82, Y=1.10834264786325, Z=2.558, q_1=0, q_2=0.1 and q_3=0.7 we can obtain $\det(\boldsymbol{J}^T)=1.91331247739506\times10^{-13}$. This singular configuration can be represented graphically as follows.

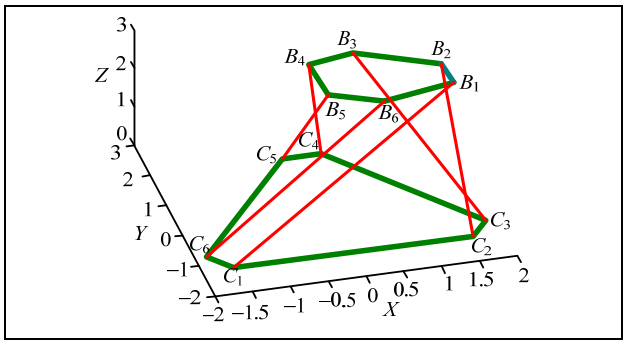

Figure 2. One singular configuration of the GSPs

The singularity locus of the GSP with six-DOF is a hypersurface embedded in six-dimensional space and is impossible to visualize. According to [12], the task space of the moving platform of the parallel mechanism with six-DOF is a configuration space, which also corresponds to $SE(3)$. Here $SE(3)$ represents the group operation of the

pose (position and orientation) of a rigid body, which corresponds to the semi-direct product of the three-dimensional rotation group and the three-dimensional Euclid space, i.e., $SE(3)=SO(3) \otimes \Re^3$. Therefore, we can classify the singularity of the mechanism into two types in the configuration space in $SE(3)$ considering the representation form of the parameters: the position-singularity in $\Re^3$ for a constant- orientation and the orientation-singularity in $SO(3)$ for a given position. Then the singularity locus of the GSP in the configuration space can be represented easily in $\Re^3$ and in $SO(3)$, respectively.

4.1 Position-singularity representation

According to Equation (4), a cubic symbolic expression in terms of variables (X, Y, Z) representing the position-singularity locus in $\Re^3$ for a constant-orientation (q_1, q_2, q_3) can be written as

$$f_1Z^3 + f_2XZ^2 + f_3YZ^2 + f_4X^2Z + f_5Y^2Z + f_6XYZ + f_7Z^2 + f_8XZ + f_9YZ + f_{10}X^2 + f_{11}XY + f_{12}Y^2 + f_{13}Z + f_{14}X + f_{15}Y + f_{16} = 0 \quad , \tag{5}$$

where f_i (i =1, 2, …, 16) are all functions in terms of the geometry parameters R_m, R_b, β_m, β_b and the orientation parameters (q_1, q_2, q_3).

The graphical representation of the position-singularity locus in $\Re^3$ for a constant-orientation is shown in Figure 3 Here the geometry parameters are given as R_m = 1, R_b = 2, β_m = 75° and β_b = 105°, and the orientation parameters are (0, 0.1, 0.7).

Equation (5) shows that the position-singularity equation of the mechanism for a constant-orientation is a polynomial expression of three degrees in terms of the position parameters (X, Y, Z) and the maximum degree of X, Y is two and Z is three. Figure 3 shows that the position-singularity surface of the mechanism for a constant-orientation is rather complicated and quite variable. Some researchers obtained a quadratic polynomial of Equation (5) and gave the geometric characteristics of the position-singularity locus for a constant-orientation in some special sections. By using the standard ZYZ-Euler angles to describe the orientation of the moving platform of the mechanism, Huang et al. [17], transformed the cubic position-singularity equation into the characteristic coordinate system in the platform plane into a quadratic equation, which indicated the geometric characteristics of the position-singularity locus in the oblique platform plane. Then Li et al. [18], further advanced two theorems about the geometric characteristics of the position- singularity locus in the oblique platform plane, which was called the "characteristic plane". Bandyopadhyay et al. [19] obtained a quadratic polynomial of the position-singularity expression when the parameter Z is given, which shows the position-singularity locus of the moving platform in the plane parallel to the base platform with height Z.

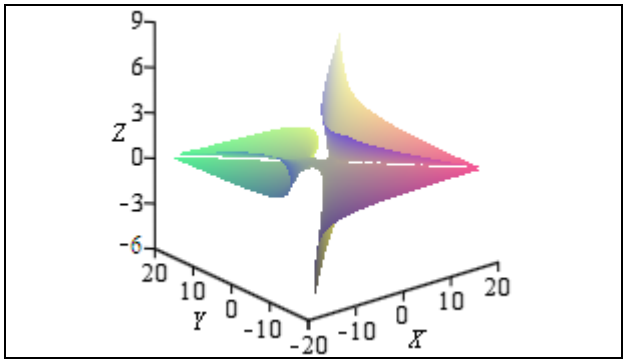

Figure 3. Position-singularity locus for the constant-orientation (0, 0.1, 0.7)

4.2 Orientation-singularity representation

Supposing that the position variables are given, Equation (4) yields the orientation-singularity expression indicating the orientation-singularity locus of the mechanism for a given position, which is shown as follows

$$f_1q_1^6 + f_2q_1^5q_2 + f_3q_1^5q_3 + f_4q_1^5\sqrt{1-q_1^2-q_2^2-q_3^2} + \cdots + f_{69}q_2^2 + f_{70}q_2q_3 + f_{71}\sqrt{1-q_1^2-q_2^2-q_3^2} + f_{72}q_3^2 + f_{73} = 0 . \tag{6}$$

where, coefficients f_i(i=1, 2, …, 73) are all functions in terms of the geometry parameters R_m, R_b, β_m, β_b and the position parameters (X, Y, Z). Further inspection shows that Equation (6) has many terms including $\sqrt{1-q_1^2-q_2^2-q_3^2}$ and the highest degree of the orientation parameters (q_1, q_2, q_3) is six. Therefore the orientation-singularity expression is very complex. It can also be shown that the orientation-singularity expression is more complicated than the position-singularity expression.

When the geometry parameters are given as R_m=1, R_b=2, β_m=75° and β_b=105°, the graphical representation of the orientation-singularity locus in $SO(3)$ with respect to (q_1, q_2, q_3) in the Cartesian coordinates for the given position (0, 0, 3.5) is given as an example to illustrate the result, as shown in Figure 4.

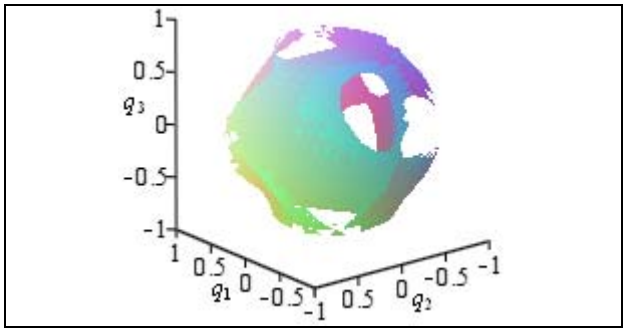

Figure 4. Orientation-singularity locus for the given position (0, 0, 3.5)

5. Workspace determination

When the initial installation of the mechanism is just finished, the pose of the moving platform is called the "initial pose", where the position parameters (X, Y, Z) are always (0, 0, Z_0) and the orientation parameters (q_1, q_2, q_3) are always (0, 0, 0), and where Z_0 can be obtained according to Subsection 5.2.2. After substituting q_1=0, q_2=0 and q_3=0 into Equation (4), the singularity expression for the constant-orientation (0, 0, 0), which does not include the items X and Y, can be obtained as

$$gZ^3 = 0, \tag{7}$$

where g is the function in terms of the geometry parameters R_b, R_m, β_b, β_m and is not equal to zero when $\beta_b+\beta_m\neq120°$. The orientation (0, 0, 0) will be defined as the "central orientation" in Section 5.4. Equation (7) is true only if Z=0. That is to say, if the position parameter Z is not zero and whatever the position parameters X, Y are, the mechanism is non-singular for the orientation (0, 0, 0). Moreover, the left side of Equation (4), the determinant of the matrix $\boldsymbol{J}^T$, is a continuous function in terms of the position parameters (X, Y, Z) and the orientation parameters (q_1, q_2, q_3). Therefore, when the moving platform moves in the workspace, the sign on the left side of Equation (4) for any pose (position and orientation) parameters must be the same as the sign on the left side of Equation (7) for Z=Z_0, so as to guarantee the mechanism is non-singular with the configuration of the mechanism changing.

In practice, the movement of the moving platform from the current pose (position and orientation) to the desired pose can usually be divided into two steps: translating from the current position to the desired position first and then rotating to the desired posture. Similarly to the singularity representation of the mechanism, we can describe the position-workspace (constant-orientation workspace) in three-dimensions and the orientation workspace (constant-position workspace) in three-dimensions instead of giving a complete representation of the workspace in six-dimensions. Furthermore, the "constraint position-workspace" and the "constraint orientation-workspace" are proposed here considering the kinematic constraints of the mechanism. The "constraint position-workspace" is the three- dimensional position zone where the moving platform can reach for a constant orientation posture taking the restrictions of the kinematic pairs and the singularities into consideration. The "constraint orientation- workspace" is the three-dimensional orientation void where the moving platform can rotate for a given position posture taking the kinematic constraints and the singularities into consideration. As has been stated, the PM's closed loop nature may create complex singularities inside the constraint workspace. Therefore, we also propose a "non-singular position-workspace" and a "non-singular orientation-workspace". When the moving platform translates inside the three-dimensional zone called the "non-singular position-workspace" for a constant-orientation, the mechanism is non-singular when considering the restriction of the kinematic pairs. Similarly, when the moving platform rotates inside the three-dimensional "non-singular orientation-workspace" for a given position, the mechanism is non-singular when taking the restriction of the kinematic pairs into consideration. New algorithms for determining the aforementioned several types of the workspace, i.e., the constraint position workspace, the non-singular position workspace, the constraint orientation workspace and the non-singular orientation workspace of the GSP will be represented based on the inverse kinematics of the mechanism when considering the kinematic constraints.

5.1 Inverse kinematics

The starting point of the workspace of the mechanism analysis is the solution of the inverse kinematics. Given a pose of the moving platform, the ith link vector, denoted by $\boldsymbol{l}_i$, can be computed by the following formula

$$\boldsymbol{l}_i = \boldsymbol{B}_i - \boldsymbol{C}_i \quad (i=1, 2, \ldots, 6), \tag{8}$$

where the meaning of $\boldsymbol{B}_i$ and $\boldsymbol{C}_i$ are illustrated in Section 3.2 and l_i represents the length of the ith actuator and can be calculated by the following expression

$$l_i = |l_i| = |\boldsymbol{B}_i - \boldsymbol{C}_i| \quad (i=1, 2, \ldots, 6). \tag{9}$$

5.2 Kinematic constraints

There are three types of main kinematic constraints: the actuators' stroke, the range of passive joints and the link interference.

5.2.1 Actuators' stroke

The limited stroke of the ith actuator imposes a link-length constraint on the ith prismatic joint, that is

$$L_{\min} \le l_i \le L_{\max} \quad (i=1, 2, \ldots, 6), \tag{10}$$

where $L_{\min}$ and $L_{\max}$ are the minimum and maximum lengths of the actuators, respectively.

5.2.2 Range of passive joints

Let $\theta_{B\max i}$ and $\theta_{C\max i}$ be the range of the ith passive joints B_i and C_i, respectively. We can obtain

$$\theta_{Bi} = \arccos\frac{\boldsymbol{l}_i \cdot (\boldsymbol{R}\boldsymbol{l}_{ni})}{|\boldsymbol{l}_i| \cdot |\boldsymbol{l}_{ni}|}, \tag{11}$$

$$\theta_{Ci} = \arccos \frac{\boldsymbol{l}_i \cdot \boldsymbol{l}_{ni}}{|\boldsymbol{l}_i| \cdot |\boldsymbol{l}_{ni}|}, \quad (12)$$

where $\boldsymbol{R}$ is the rotation matrix, as Equation (1) shows. $\boldsymbol{l}_{ni}$ is the ith actuator's vector with respect to the fixed reference, where all of the lengths of the six actuators are $0.5(L_{min}+L_{max})$ for the initial pose of the moving platform. Substitute the initial pose parameters (X, Y, Z)=(0, 0, Z_0) and (q_1, q_2, q_3)= (0, 0, 0) into Equation (2) and compute the length of any one actuator determined by Equation (9). Set

$$l_i = |\, l_i \,| = |\, \boldsymbol{B}_i - \boldsymbol{C}_i \,| = 0.5(L_{min}+L_{max}),$$

where $l_i = l_j$ (i, j=1, 2, …, 6). Then the following function in terms of one variable Z_0 can be obtained

$$\sqrt{Z_0^2 + g_0} = 0.5(L_{min}+L_{max}), \quad (13)$$

where g_0 is determined by the geometric parameters of the mechanism R_b, R_m, β_b, β_m. Equation (13) has two real roots with the same absolute value and the opposite sign. Here we set $Z_0 > 0$ with considering the case that the moving platform only works in the zone on the topside of the base platform, as shown in Figure 1. Substitute the initial pose parameters (0, 0, Z_0, 0, 0, 0) into Equation (2), then $\boldsymbol{l}_{ni}$ can be derived easily by employing Equation (8) but is not given here because of the limited space.

5.2.3 Link interference

Supposing that each actuator can be approximated by a cylinder of diameter D and the distance between two adjacent actuators are $D_{i,\,i+1}$ (i, i+1=1, 2, …, 6), which imposes a constraint on the relative position of all pairs of actuators, such that

$$D \le D_{i,\,i+1} \quad (i=1, 2, \ldots, 6). \quad (14)$$

The method for computing $D_{i,\,i+1}$ is addressed in [9] and is not represented here because of the limited space.

According to the inverse kinematics and computation of the changes of the joints, the constraint position-workspace and the constraint orientation-workspace can be obtained. Then the non-singular position-workspace and the non-singular orientation-workspace can further be represented by analysing the distribution of the position- singularity locus inside the workspace. In order to clearly address the process, the algorithms of the constraint workspace and the non-singular workspace will be represented by giving numerical examples. The design parameters of the mechanism under investigation are given in Table 1 where the initial position parameter Z_0 can be obtained as 3.80 by solving Equation (13) in terms of one variable Z_0.

β_m (°)	β_b (°)	R_m (m)	R_b (m)	L_{min} (m)	L_{max} (m)	θ_{Bmax} (°)	θ_{Cmax} (°)	D (m)
75	105	1	2	3	5	55	55	0.15

Table 1. Design parameters of the GSP under investigation

5.3 Position-workspace determination

Masory [20] and Huang [9] introduced a quick radial search to determine the boundary of the position-workspace of the GSP. However, using this algorithm it is very difficult to find out the boundary of the position-workspace with more than one zone and voids located inside the position-workspace. Moreover, the centre of the position-workspace should be located when using the radical search, but the centre generally cannot be located easily. This section will propose a new algorithm for finding out the boundary of the position-workspace of the GSP for a constant-orientation. The new algorithm for determining the constraint position-workspace and the non-singular position-workspace of the mechanism is developed by combining the step-by-step search and the bisection method. First, the position-workspace boundaries determined by the limitation of every kinematic pair should be found out. Then, the intersection of the position-workspaces determined by all limitations of the kinematic pairs is used as the constraint position-workspace. Finally, the non-singular position-workspace can be obtained by finding out the singularities inside the constraint position-workspace. The process is represented as follows:

(1) Substitute the geometry parameters R_b, R_m, β_b, β_m and the initial pose parameters (X, Y, Z, q_1, q_2, q_3)=(0, 0, Z_0, 0, 0, 0) into the left side of Equation (4) which is denoted by $F(\mathscr{A}, \mathscr{B})$.

(2) Divide the possible reachable position-workspace for a constant-orientation into different slices by step ΔZ, as Figure 5 shows.

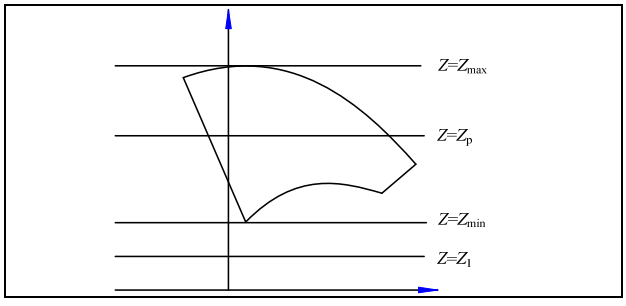

Figure 5. Slices of the position-workspace

(a) Transform the position parameters (X, Y) into the polar form and choice any one position (X_P, Y_P) as the starting point:

$$X = \rho\cos\alpha + X_P$$
$$Y = \rho\sin\alpha + Y_P \quad (15)$$

where (X_P, Y_P) can be set as (0, 0) when the centre of the position-workspace in the Z-section is not known. When in the slice of $Z=Z_P$, substitute Equation (15) into Equation (5), which yields an expression with variables α and ρ

$$F(\rho, \alpha)=0. \tag{16}$$

(b) Discretize α and ρ by step $\Delta\alpha$ and $\Delta\rho$, respectively

$$\alpha_{j+1}=\alpha_j+\Delta\alpha \quad (j, j+1=1, 2, \ldots, 2\pi/\Delta\alpha),$$
$$\rho_{k+1}=\rho_k+\Delta\rho \quad (k, k+1=1, 2, \ldots, \rho_{max}/\Delta\rho),$$

where $\alpha_1=0$, $\rho_1=0$ and ρ_{max} is the maximal radius of the radial search. ρ_{max} should be long enough so as to find out all of the possible position-workspace boundaries in the Z-section and can be estimated according to the design parameters of the mechanism.

(c) Substitute the geometry parameters R_m, R_b, β_m, β_b and the orientation parameters q_1, q_2, q_3 into the kinematic constraint equations as follows:

$$L_i-L_{min}=0 \quad (i=1, 2, \ldots, 6) \tag{17}$$
$$L_i-L_{max}=0 \quad (i=1, 2, \ldots, 6) \tag{18}$$
$$\theta_{Bi}-\theta_{Bmax}=0 \quad (i=1, 2, \ldots, 6) \tag{19}$$
$$\theta_{Ci}-\theta_{Cmax}=0 \quad (i=1, 2, \ldots, 6) \tag{20}$$
$$D_{i, i+1}-D_{min}=0 \quad (i=1, 2, \ldots, 6) \tag{21}$$

(3) For one subspace of the slices, the constraint position-workspace, taking kinematic constraints into consideration, can be searched by the following steps (3a)-(3f) using the radial search combining the bisection method and the step-by-step search.

(a) Set $\alpha=\alpha_j$ (j=1, 2, …, $2\pi/\Delta\alpha$), increase ρ from 0 by step $\Delta\rho$ and substitute ρ_k and α_j into Equation (9), whose value is denoted by $L(\rho_k)$. Set m=0.

(b) If $L_i(\rho_k)=L_{mini}$, ρ_k satisfies Equation (17). Denote ρ_k as $\rho(m)$, and set $m=m+1$.

(c) If $[L_i(\rho_k)-L_{min}]\times[L_i(\rho_{k+1})-L_{min}]<0$, search the root of Equation (17) in terms of variable ρ using the bisection method over the starting range $[\rho_k, \rho_{k+1}]$ and denote the root as $\rho(m)$ and set $m=m+1$. The details of the bisection method can be represented easily by referring to many textbooks about numerical computation and are not given here because of the limited space.

The boundaries of the position-workspace determined by the minimal length of the six links L_{min} as Equation (17) shown can be found out using steps (3a)-(3c).

(d) Similarly to steps (3a)-(3c), the boundary points of the position-workspace determined by L_{max}, θ_{Bmax}, θ_{Cmax} and D_{min} can also be found by searching the real root of Equations (18)-(21) in terms of variable ρ when α is set as α_j.

(e) Repeat steps (3a)-(3d), substitute $\rho(m)$ and the corresponding α_j into Equation (15), then the position of the boundaries points of the position-workspace determined by the limitations of the kinematic pairs can be obtained as

$$\begin{aligned} X(m)&= \rho(m)\cos\alpha_j+X_P \\ Y(m)&=\rho(m)\cos\alpha_j+Y_P \\ Z(m)&=Z_P \end{aligned} \tag{22}$$

Thus the constraint position-workspace boundaries points determined by L_{max}, L_{min}, θ_{Bmax}, θ_{Cmax} and D_{min} can be obtained, respectively.

For example, if Z=3, when the orientation parameters are given as (0, 0.1, 0.7), the constraint position-workspace boundaries determined by the limitations of the kinematic pairs are represented as shown in Figure 6. Here ρ_{max} is set as six, which is enough to search the possible boundaries considering the restrictions of the kinematic pairs. From Figure 6, it can be shown that when the design parameters are given as shown in Table 1 and the orientation parameters are (0, 0, 0.7), link interference will not occur because of the limitations of the kinematic pairs.

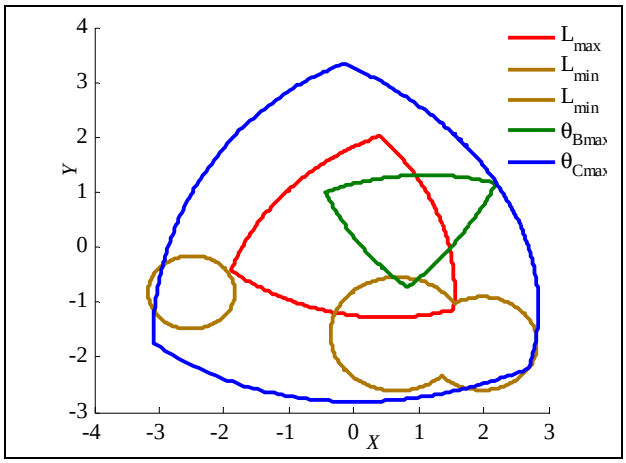

Figure 6. Constraint position-workspace boundaries determined by limitations of the kinematic pairs

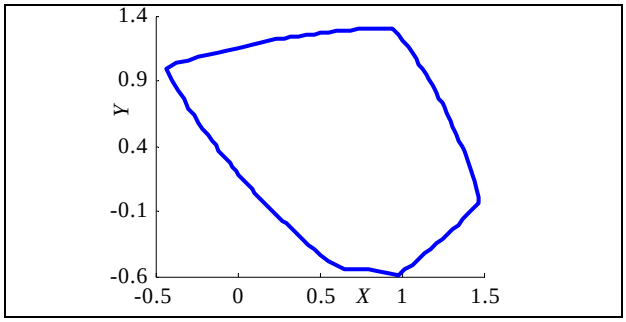

Figure 7. Constraint position-workspace in the Z-section when Z=3

(f) Substitute the set of the position parameters ($X(m)$, $Y(m)$, $Z(m)$) into Equation (2) and then calculate the length of the six links l_i using Equation (9), the rotated angle of the passive joints θ_{Bi}, θ_{Ci} using Equations (11, 12)

and the shortest distance between two adjacent actuators $D_{i,i+1}$ addressed in [9]. If l_i, θ_{Bi}, θ_{Ci} and $D_{i,i+1}$ satisfy

$$L_{min} \le l_i \le L_{max}, \quad (23)$$

$$\theta_{Bi} \le \theta_{Bmax}, \quad (24)$$

$$\theta_{Ci} \le \theta_{Cmax}, \quad (25)$$

$$D_{i,i+1} \ge D_{min}, \quad (26)$$

respectively, the searched $X(m)$, $Y(m)$ and $Z(m)$ are the boundary points of the position-workspace of the mechanism for constant-orientation in the Z-plane considering the kinematic constraints. After carrying out Step (3f), the constraint position-workspace boundary in the Z-section can be obtained as shown in Figure 7.

Figure 8 further shows the position-singularity curves in the Z-section. It can be found out that the singularities exist inside the constraint position-workspace. Therefore, the non-singular position-workspace should be determined in order to avoid the singularities. Figure 9 shows the constraint position-workspace in another Z-section when Z=2.675. It can be shown that the algorithm proposed here is also applicable to searching the boundaries of the constraint position-workspace with more than one zone. Moreover, the developed process is also efficient in searching the position-workspace whose centre is not known. Therefore, the algorithm addressed here is more efficient than the general radical search and can also be used to determine the position-workspace of other types of parallel mechanisms.

(4) Find out the non-singular boundary points of the constraint position-workspace.

Substitute the obtained $X(m)$, $Y(m)$, $Z(m)$ to the left side of Equation (5) denoted by $F[X(m), Y(m), Z(m), q_1, q_2, q_3]$, where (q_1, q_2, q_3) is the given constant orientation parameters. If $F[X(m), Y(m), Z(m)]\times F(\mathscr{A}, \mathscr{B}) \ge 0$, the obtained $X(m)$, $Y(m)$ and $Z(m)$ can be used as the boundary points of the non-singular position-workspace in the Z-section, where $(\mathscr{A}, \mathscr{B})$ is the initial pose parameters $(0, 0, Z_0, 0, 0, 0)$.

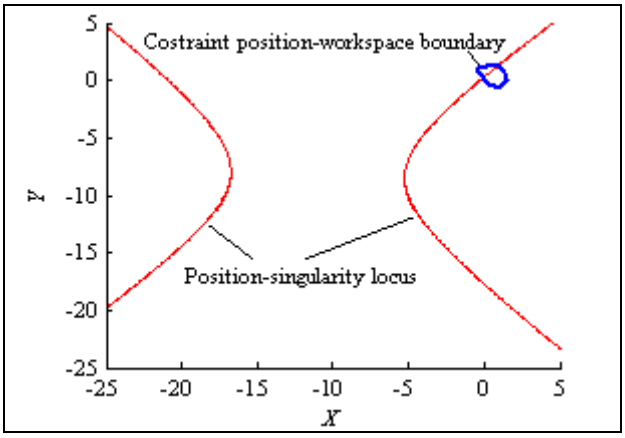

Figure 8. Constraint position-workspace and position-singularity locus in the horizontal section of Z=3

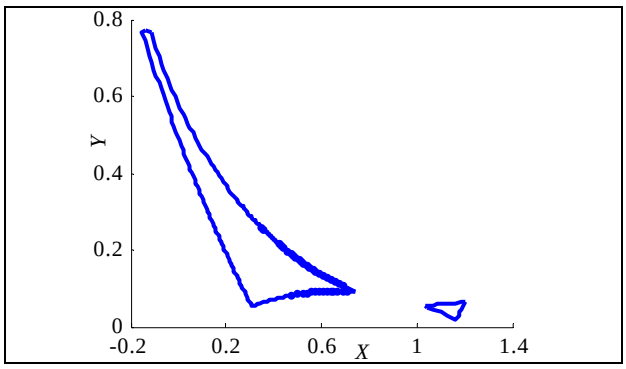

Figure 9. Constraint position-workspace in the horizontal section of Z=2.675

(5) Search the non-singular position-space boundary determined by the singularity locus in the Z-section.

(a) Set $\alpha=\alpha_j$ (i=1, 2, …, $2\pi/\Delta\alpha$), increase ρ from 0 by step $\Delta\rho$ and substitute ρ_k and α_j into the left side of Equation (16), whose value is denoted by $F(\rho_j)$. Set n=0.

(b) If $F(\rho_k)$=0, then ρ_k satisfies Equation (16). Set $\rho(n)=\rho_k$ and $n=n$+1.

(c) If $F(\rho_k)\times F(\rho_{k+1})$<0, search the root of Equation (16) in terms of ρ using the bisection method over the starting range $[\rho_k, \rho_{k+1}]$, denote the root as $\rho(n)$ and set $n=n$+1.

(d) The position-singularity points $\rho(n)$ in the polar form when $\alpha=\alpha_j$ in the Z-plane can be found out by steps (5a)-(5c), as Figure 10 shows.

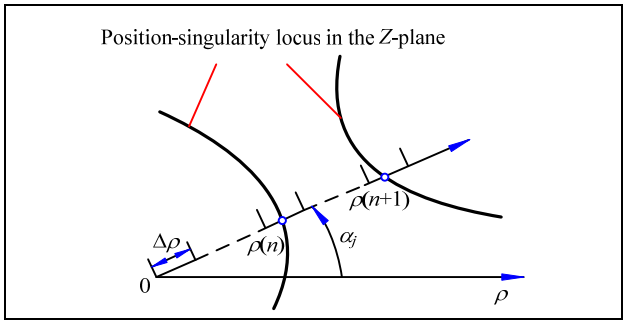

Figure 10. Notation of ρ satisfying Equation (16) when α is given in the Z-plane

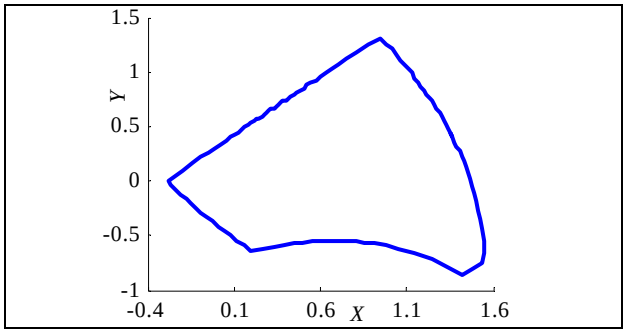

Figure 11. Non-singular position-workspace in the horizontal section of Z=3

(e) Repeat steps (5a)-(5d), substitute $\rho(n)$ and the corresponding α_j into Equation (15):

$$\begin{aligned} X(n) &= \rho(n)\cos\alpha_j + X_P, \\ Y(n) &= \rho(n)\cos\alpha_j + Y_P, \\ Z(n) &= Z_P. \end{aligned} \tag{27}$$

The calculated $X(n)$ and $Y(n)$ are the singularity points of the mechanism for a constant-orientation in the Z-plane. Substitution of the calculated $X(n)$ and $Y(n)$ to Equations (9, 11, 12) can obtain the changes of the kinematic pairs. If the changes of the kinematic pairs satisfy Equations (23)-(26), $X(n)$ and $Y(n)$ can be used as the boundary points of the non-singular position-workspace.

(6) Repeat Steps (3)-(5), the boundary points of the non-singular position-workspace in one slice of the Z-plane can be obtained, as shown in Figure 11.

(7) Determination of the three-dimensional constraint position-workspace. For every other subspace of the slices, repeat Step (3), the boundary of the three- dimensional constraint position-workspace of the mechanism for a constant-orientation can be represented. Figure 12 shows the constraint position-workspace of a specific GSP, where the design parameters are given as shown in Table 1 and the orientation parameters are given as (0, 0.1, 0.7).

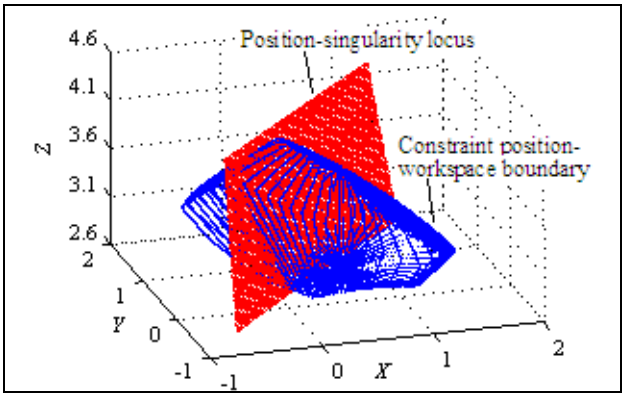

Figure 12. Constraint position-workspace inside which the singularities exist

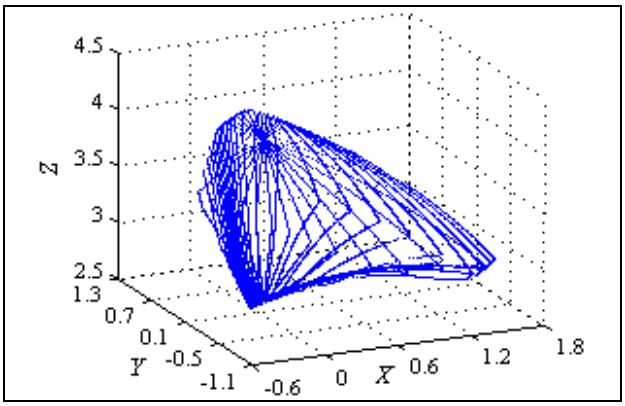

Figure 13. Non-singular position-workspace for a constant-orientation

(8) Determination of the three-dimensional non-singular position-workspace. For every other subspace of the slices, carry out Steps (3)-(6). The non-singular position-workspace of the mechanism for a constant-orientation without considering the singularity can be obtained by carrying out Steps (3)-(6). Figure 13 shows the three-dimensional non-singular position-workspace for the constant orientation (0, 0.1, 0.7), inside which no singularity exists.

5.4 Orientation-workspace determination

According to Equation (7), when the moving platform translates in the workspace with an orientation satisfying $(q_1, q_2, q_3)=(0, 0, 0)$, the mechanism will not be singular so long as $Z\neq 0$, where $Z\neq 0$ means the plane where the moving platform lies does not coincide with the plane where the fixed platform lies. Moreover, when the position of the moving platform is given, the left side of Equation (7), i.e., the determinant of the matrix $\boldsymbol{J}^T$, is a continuous function in terms of the orientation parameters (q_1, q_2, q_3). Therefore, when $Z\neq 0$, whatever the position parameters (X, Y) are, a non-singular orientation-void around the orientation origin $(q_1, q_2, q_3)=(0, 0, 0)$ can always be found. From Figure 4, it can be shown that a singularity-free void really exists around the central orientation $(q_1, q_2, q_3)=(0, 0, 0)$ and inside the orientation-singularity surface.

In this section, we will represent the algorithm of the constraint orientation-workspace and the non-singular orientation-workspace of the mechanism for a given position considering the kinematic constraints. The mechanism is not singular when the moving platform rotates inside the non-singular orientation-workspace for a given position.

We define a "central orientation" of the mechanism, which should satisfy the following two assumptions:

(1) The position of the point P is given.

(2) The orientation of the moving reference frame is the same as the orientation of the fixed one.

The process can be briefly addressed as: first, search the boundaries determined by all limitations of the kinematic pairs starting from the "central orientation". Then, use the boundary being closest to the "central orientation" as the constraint orientation-workspace boundary. In fact, if the one directional "closest boundary point" determined by the limitation of one of the kinematic pairs is found out, we can stop searching the other boundary points in the one direction determined by other limitations of the kinematic pairs. Finally, the intersection set of the singularity-free void determined by the orientation-

singularity locus and the constraint orientation-workspace is used as the non-singular orientation-workspace.

Considering $q_1^2+q_2^2+q_3^2 \le 1$, convert the unit quaternion to the following representation considering the property of the unit quaternion:

$$\begin{aligned} q_1 &= r\sin\gamma\cos\phi, \\ q_2 &= r\sin\gamma\sin\phi, \\ q_3 &= r\cos\gamma, \end{aligned} \quad \gamma\in[0,\pi],\ \beta\in[0,2\pi],\ r\in[0,1] \qquad (28)$$

Another point to note that the spherical coordinates systems is constructed here because of considering the computation convenient of the orientation capability defined as $R_{oc}=\sqrt{q_1^2+q_2^2+q_3^2}$, which will be investigated in our future work.

By synthetically using the step-by-step search and the bisection method, the algorithm of the non-singular orientation-workspace of the mechanism for a given position can be represented as follows:

(1) Search the constraint position-workspace for the "central orientation" considering the limitations of the kinematic pairs by using the algorithm proposed in Section 5.3. Then, save the set of all positions, (X, Y, Z) that can be reached by point P. The constraint orientation-workspace and the non-singular orientation-workspace for any given position, (X, Y, Z), located in this searched position-workspace can be found out by the following steps.

(2) Discretize γ, ϕ and r by step $\Delta\gamma$, $\Delta\phi$, Δr, respectively

$$\begin{aligned} \gamma_{i+1}&=\gamma_i+\Delta\gamma \quad (i,\ i+1=1,2,\ldots,\pi/\Delta\gamma) \\ \phi_{j+1}&=\phi_j+\Delta\phi \quad (j,\ j+1=1,2,\ldots,2\pi/\Delta\phi) \\ r_{k+1}&=r_k+\Delta r \quad (k,\ k+1=1,2,\ldots,1/\Delta r) \end{aligned}$$

where $\gamma_1=0$, $\phi_1=0$, $r_1=0$. γ_i, ϕ_j and the boundary point of the orientation-workspace denoted by $r_{i,j}$ are shown in Figure 14.

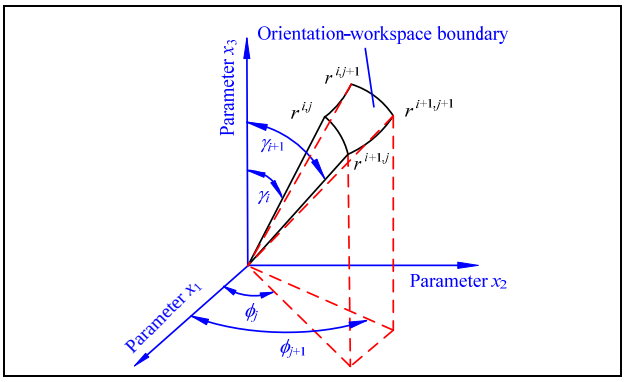

Figure 14. Notation of the boundary point of the orientation-workspace

(3) Step (3) mainly deals with the constraint orientation-workspace determined by the kinematic constraints without considering the singularities. Set $\gamma=\gamma_i$ (i=1, 2, …, $\pi/\Delta\gamma$), carry out the following Steps (a)-(f):

(a) Set $\phi=\phi_j$ (j=1, 2, …, $2\pi/\Delta\phi$), increase r from 0 by step Δr and denote value of r as λ_k. Substitute the given position parameters (X, Y, Z) and the current parameters (λ_k, γ_i, ϕ_j) into Equation (2), then solve the inverse kinematics by employing Equation (9), Equation (11) and Equation (12), which are all the functions in terms of λ_k and denoted by $L_i(\lambda_k)$, $\theta_{Bi}(\lambda_k)$, $\theta_{Ci}(\lambda_k)$, respectively.

(b) When r is set as λ_k, if any one change of the kinematic pairs satisfies the following:

$$L_i(\lambda_k)-L_{\min}=0 \qquad (29)$$
$$L_i(\lambda_k)-L_{\max}=0 \qquad (30)$$
$$\theta_{Bi}(\lambda_k)-\theta_{B\max}=0 \qquad (31)$$
$$\theta_{Ci}(\lambda_k)-\theta_{C\max}=0 \qquad (32)$$
$$D_{i,i+1}(\lambda_k)-D_{\min}=0 \qquad (33)$$

then $\lambda^{i,j}=\lambda_k$ and stop Step (3b).

(c) If the changes of the kinematic pairs satisfy any one of the following:

$$\begin{gathered} [L_i(\lambda_k)-L_{\min}]\times[L_i(\lambda_{k+1})-L_{\min}]<0 \\ [L_i(\lambda_k)-L_{\max}]\times[L_i(\lambda_{k+1})-L_{\max}]<0 \\ [\theta_{Bi}(\lambda_k)-\theta_{B\max}]\times[\theta_{Bi}(\lambda_{k+1})-\theta_{B\max}]<0 \\ [\theta_{Ci}(\lambda_k)-\theta_{C\max}]\times[\theta_{Ci}(\lambda_{k+1})-\theta_{C\max}]<0 \\ [D_{i,i+1}(\lambda_k)-D_{\min}]\times[D_{i,i+1}(\lambda_{k+1})-D_{\min}]<0 \end{gathered}$$

then $\lambda^{i,j}\in(\lambda_k,\ \lambda_{k+1})$. Thus the boundary point of the orientation-workspace $\lambda^{i,j}$ for γ_i and ϕ_j can be searched by using the bisection method over the starting range $[\lambda_k,\ \lambda_{k+1}]$ to find out the real root of the corresponding equation as Equations (29)-(33) show, respectively. After this search, stop Step (3c).

(d) If for all values of λ_k

$$\begin{gathered} [L_i(\lambda_k)-L_{\min}]\times[L_i(\lambda_{k+1})-L_{\min}]>0 \\ [L_i(\lambda_k)-L_{\max}]\times[L_i(\lambda_{k+1})-L_{\max}]>0 \\ [\theta_{Bi}(\lambda_k)-\theta_{B\max}]\times[\theta_{Bi}(\lambda_{k+1})-\theta_{B\max}]>0 \\ [\theta_{Ci}(\lambda_k)-\theta_{C\max}]\times[\theta_{Ci}(\lambda_{k+1})-\theta_{C\max}]>0 \\ [D_{i,i+1}(\lambda_k)-D_{\min}]\times[D_{i,i+1}(\lambda_{k+1})-D_{\min}]>0 \end{gathered}$$

then denote $\lambda^{i,j}=1$.

(e) Repeat Steps (a)-(d) for every other value of ϕ.

(f) Repeat Steps (a)-(e) for every other value of γ.

(4) Step (4) mainly finds out the orientation-singularity-free void determined by the orientation-singularity locus, which can be found out by following Steps (a)-(h):

(a) After substituting Equation (28) into Equation (6), the following expression with three variables r, γ and ϕ can be obtained

$$F(r, \gamma, \phi)=0. \quad (33)$$

(b) Set $\gamma=\gamma_i$ (i=1, 2, …, $\pi/\Delta\gamma$).

(c) Set $\phi=\phi_j$ (j=1, 2, …, $2\pi/\Delta\phi$), increase r from 0 by step Δr and here denote the value of r as R_k. Substitute R_k, γ_i and ϕ_j into the left of Equation (33), whose value is denoted by $F(R_k)$. If $F(R_k)\times F(R_{k+1})\leq 0$ or R_k=1, stop Step (3c).

(d) If $F(R_k)\times F(R_{k+1})=0$, $R^{i,j}=R_{k+1}$.

(e) If $F(R_k)\times F(R_{k+1})<0$, then $R^{i,j}\in(R_k, R_{k+1})$. Therefore, searching $R^{i,j}$ solves Equation (33) in terms of the real variable R, where $R\in(R_k, R_{k+1})$. The bisection method over starting range $[R_k, R_{k+1}]$ can be applied to find the real root.

(f) If for all values of R_k, $F(R_k)\times F(R_{k+1})>0$, then $R^{i,j}=1$. In this case, Equation (33) for the variable r has no real root when $\gamma=\gamma_i$ and $\phi=\phi_j$.

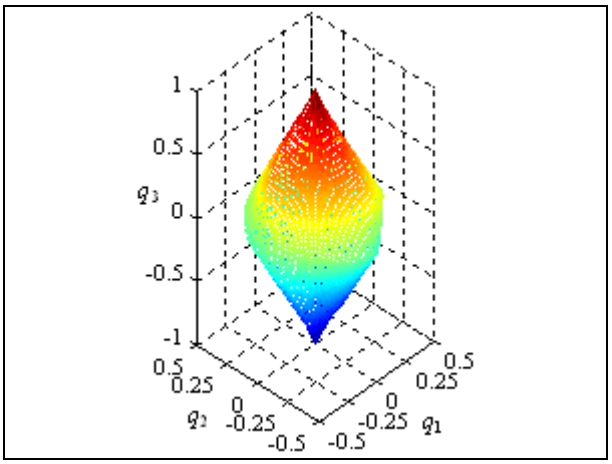

(a)Constraint orientation-workspace

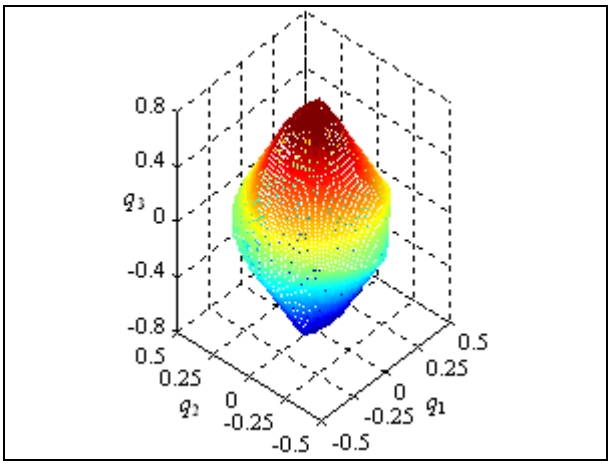

(b) Non-singular orientation-workspace

Figure 15. Orientation-workspace for a given position (0, 0, 3.5)

(g) Repeat Steps (a)-(f) for every other value of ϕ.

(h) Repeat Steps (a)-(g) for every other value of γ.

(5) When $\gamma=\gamma_i$ and $\phi=\phi_j$, take the minor value of $\lambda^{i,j}$ searched by Step (3) and $R^{i,j}$ searched by Step (4) as the boundary point of the non-singular orientation-workspace denoted by $r^{i,j}$, i.e., $r^{i,j}=\min(\lambda^{i,j}, R^{i,j})$. Thus the boundary points of the non-singular orientation-workspace in three-dimensions can be computed by using Equation (28). If set $r^{i,j}=\lambda^{i,j}$, the constraint orientation-workspace for a given position can be represented by using Equation (28).

After carrying out Steps (1)-(5), the constraint orientation-workspace and the non-singular orientation-workspace can be described easily. For example, when the architecture parameters of the GSP are given as in Table 1, Figure 15 describes the constraint orientation- workspace and the non-singular orientation-workspace of the mechanism for a given position (0, 0, 3.5). Figure 16 further shows the constraint orientation-workspace and the orientation-singularity locus in the two vertical sections when q_1=0 and q_2=0, respectively. It can be shown that the orientation-singularity locus may exist inside the constraint orientation-workspace.

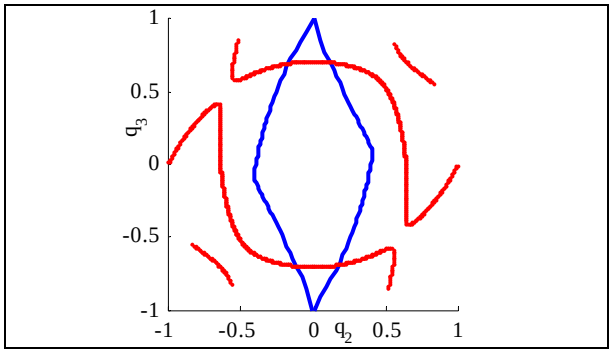

(a) Vertical section of q_1=0

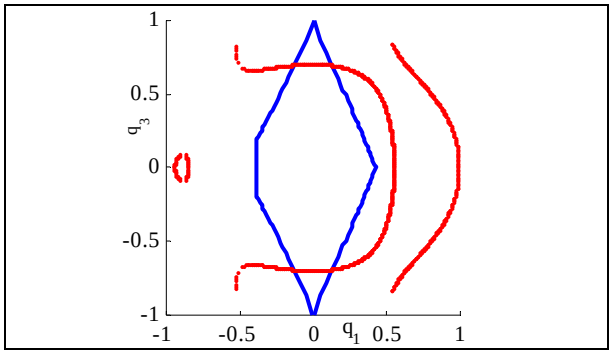

(b) Vertical section of q_2=0

Figure 16. Constraint orientation-workspace and orientation-singularity locus in the two vertical sections

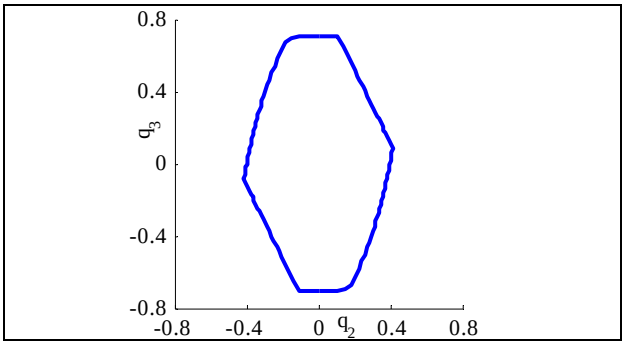

(a) Vertical section of q_1=0

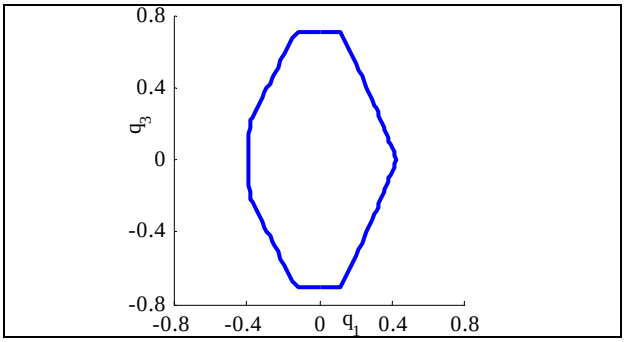

(b) Vertical section of q_2=0

Figure 17. Non-singular orientation-workspace in the two different vertical sections

Figure 17 shows the non-singular orientation-workspace in the two vertical sections when q_1=0 and q_2=0, respectively. From Figures 15-17, it can be concluded that the algorithm addressed here can certainly find out the rotation space of the mechanism for a given position when considering the restriction of the kinematic joints. The developed process can further search the non-singular orientation-workspace, inside which the mechanism is not singular when the moving platform rotates.

It should be pointed out that the orientation-workspace size can be precisely represented based on the unit quaternion representation but applying the Euler angles as the orientation parameters. For example, when the moving platform rotates parallel to the base platform, only one set of parameters (0, 0, q_3) can correctly describe the orientation. However, when using the standard *zyz*-Euler angles (ϕ, θ, ψ) to describe the orientation, if $\phi+\psi$=constant, then more than one set of parameters (ϕ, θ, ψ) can equivalently represent the orientation of the moving platform. Similarly, the other Euler angles are not avoid the singularity in parameterization, which is not illustrated here because of the limited space.

The algorithm of the workspace determination is programmed by applying Matlab 7.0 and run in Windows XP SP3, CPU Pentium Dual 2.0 GHz and RAM 2.0 GHz. It can be found that the algorithm synthetically using the step-by-step search and the bisection method is more efficient than the general radical search. For instance, when the design parameters of the mechanism are given as in Table 1, determining one section of the position-workspace boundary, where Z=3, $\Delta\rho$=0.01 and the accuracy of the boundary points is set as 10^{-10}, the computation cost is about 392 seconds using the algorithm proposed here. However, there is a computation cost of about 4105 seconds using the general radical search, where the accuracy of the boundary points is set as 10^{-3}. Therefore, the algorithms for searching the position-workspace proposed here are more efficient than the general radical search. Further investigation shows that, for other given design parameters and posture parameters, the procedure for either position-workspace determination or orientation-workspace determination addressed here is more efficient than the general radical search.

6. Conclusions

(1) From the two types of the singularity representations in $\Re^3$ and in $SO(3)$, it can be shown that the orientation-singularity locus $SO(3)$ is more complicated than the position-singularity locus in $\Re^3$.

(2) From the workspace descriptions in $\Re^3$ and in $SO(3)$, it can be concluded that the constraint orientation-workspace and the non-singular orientation-workspace in $SO(3)$ for a given position must be around the "central orientation", where the "central orientation" is where the orientation parameters are (0, 0, 0). However, the location of the position-workspace in $\Re^3$ for a constant-orientation cannot be predicted until its boundary is found out.

(3) The modified radical search by synthetically using the step-by-step search and the bisection method is a proper and efficient process for computing the three-dimensional position-workspace in $\Re^3$ and the three-dimensional orientation-workspace in $SO(3)$ of the GSP. The new algorithm is more efficient than the general radical search. Especially the algorithm proposed in this paper, which is very applicable to the search of the work zone with an arbitrary complicated shape, which may have voids and more than one zone.

(4) The concepts and algorithms of the "constraint workspace" and the "non-singular workspace" are very significant. The singularities may exist inside the constraint workspace determined by the limitations of the kinematic pairs, but do not exist inside the non-singular workspace when further considering the singularities. When the moving platform translates inside the non-singular position-workspace for a constant orientation or rotates inside the non-singular orientation-workspace for a given position, the parallel mechanism is not singular.

(5) The singularity representation and the non-singular workspace determination in this paper can be used to investigate the singularity avoidance of the GSP. Based on the exploration in this paper, our future work will focus on the optimal path planning in *SE*(3) without singularity of the GSP.

7. Acknowledgments

This project is supported by the National Natural Science Foundation of China (no. 50905075), the Anhui Provincial Natural Science Foundation of China (no. 1308085QE78), the Qinglan Project of Jiangsu Province, the Fundamental Research Funds for the Central Universities (no. JUSRP51316B), the Open Project of the State Key Laboratory of Robotics and System of China (no. SKLRS-2012-MS- 07), the Open Project of the State Key Laboratory of Fluid Power and Mechatronic Systems of China (no. GZKF-201105), the Jiangsu Provincial Graduate Research and Innovation Program of China (no. CXZZ11_0482), as well as the Doctor Candidate Foundation of Jiangnan University (no. JUDCF11014).

8. References

[1] J. P. Merlet (1994) Trajectory verification in the workspace for parallel manipulators. *International Journal of Robotics Research*, 13(4): 326–333

[2] B. Dasgupta, T. S. Mruthyunjaya (1998) Singularity-free path planning for the Stewart platform manipulator. *Mechanism and Machine Theory*, 33(6),:711–725

[3] A. K. Dash, I. Chen, S. H. Yeo, G. Yang (2005) Workspace generation and planning singularity-free path for parallel manipulators. *Mechanism and Machine Theory*, 40(7): 776–805

[4] V. Glazunov (2006) Twists of movements of parallel mechanisms inside their singularities. *Mechanism and Machine Theory*, 41(10): 1185-1195

[5] V. Arakelian, S. Briot, V. Glazunov (2007) Improvement of functional performance of spatial parallel manipulators using mechanisms of variable structure. *Proceedings of the Twelfth World Congress in Mechanism and Machine Science IFToMM*, Besancon, France, June 18-21: 159-164

[6] J. Saglia, J. S. Dai, D. G. Caldwell (2008) Geometry and kinematic analysis of a redundantly actuated parallel mechanism that Eliminates Singularity and Improves Dexterity. *ASME, Journal of Mechanical Design*, 130(12): 124501_1–5

[7] Y. X. Wang, Y. T. Li, S. X. Pan (2008) A novel method of avoiding the turning point singularity problem of parallel mechanisms. (in Chinese). *Science China: Technological Sciences*, 38(1): 125–136

[8] D. Stewart (1965) A platform with six degrees of freedom. *Proceedings of the Institution of Mechanical Engineers*, 180(5): 371–378

[9] Z. Huang, Y. S. Zhao, T. S. Zhao (2005) Advanced Spatial Mechanism. *Higher Education Press*, Beijing, China

[10] H. Li, C. M. Gosselin, M. J. Richard (2007) Determination of the maximal singularity-free zones in the six-dimensional workspace of the general Gough–Stewart platform. *Mechanism and Machine Theory*, 42(4): 1281–1293

[11] Q. Jiang, C. M. Gosselin (2009) Determination of the maximal singularity-free orientation workspace for the Gough-Stewart platform. *Mechanism and Machine Theory*, 44(6): 1281–1293

[12] R. M. Murray, Z. Li, S. S. Sastry (1994) A Mathematical introduction to robotic manipulation. Boca Raton: *CRC Press*

[13] Z. Huang, Y. Y Qu (1987) The analysis of the special configuration of the spatial parallel manipulators. (in Chinese). *The 5th National Mechanism Conference*, Lu Shan, China: 1–7

[14] C. M. Gosselin, J. Angeles (1990) Singularity analysis of closed-loop kinematic chains. *IEEE Transactions on Robotics and Automation*, 6(3): 281–290

[15] B. M. St-onge, C. M. Gosselin (2000) Singularity analysis and representation of the general Gough-Stewart platform. *International Journal of Robotics Research*, 19(3): 271–288

[16] O. Ma, J. Angeles (1991) Architecture singularities of platform manipulators. *Proceedings of the IEEE International Conference on Robotics and Automation*, Sacramento, California, 1542–1547

[17] Z. Huang, Y. Cao (2005) Property Identification of the singularity loci of a class of the Gough-Stewart manipulators. *International Journal of Robotics Research*, 24(8): 675–685

[18] B. Li, Y. Cao, Q. J. Zhang, Z. Huang (2013) Position-singularity analysis of a special class of the Stewart parallel mechanisms with two dissimilar semi-symmetrical hexagons. *Robotica*, 31(1): 123–136

[19] S. Bandyopadhyay, A. Ghosal (2006) Geometric characterization and parametric representation of the singularity manifold of a 6-6 Stewart platform manipulator. *Mechanism and Machine Theory*, 11(41): 1377–1400

[20] O. Masory, J. Wang (1995) Workspace evaluation of Stewart platforms. *Advanced Robotics*, 9(4): 443–461